ACS OMEGA

http://pubs.acs.org/journal/acsodf

Article

Fabrication of a Three-Dimensionally Networked MoO_3/PPy/rGO Composite for a High-Performance Symmetric Supercapacitor

Hangchun Deng, Jie Huang, Zhiyong Hu, Xiangfei Chen, Dejuan Huang,* and Tianxiang Jin*

Cite This: *ACS Omega* 2021, 6, 9426−9432

Read Online

ACCESS | Metrics & More | Article Recommendations

ABSTRACT: A three-dimensionally interconnected molybdenum trioxide (MoO_3)/polypyrrole (PPy)/reduced graphene oxide (rGO) composite was synthesized via an eco-friendly three-step method. The as-obtained electrode shows a high specific capacity of 412.3 F g^{-1} at a current density of 0.5 A g^{-1} and a good cycling stability (85.1% of the initial specific capacitance after 6000 cycles at 2 A g^{-1} is retained), and these excellent electrochemical performances can be attributed to the unique structure, remarkable electrical conductivity, and the synergetic effects between MoO_3, PPy, and rGO. Furthermore, a symmetric supercapacitor based on a MoO_3/PPy/rGO electrode was assembled to investigate the practical application performance of this material. The results demonstrate a high energy density of 19.8 W h kg^{-1} at a power density of 301 W kg^{-1}. These findings shine a light on the rational design of electrode materials with multicomponents for high-performance supercapacitors.

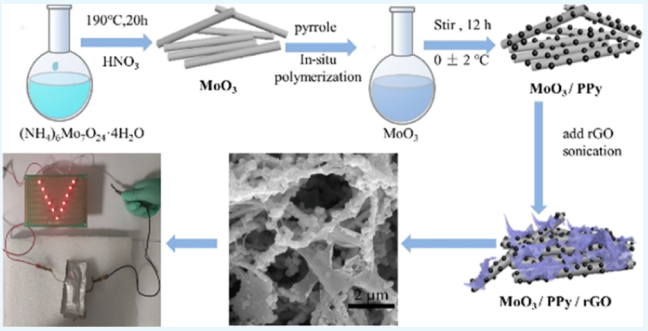

1. INTRODUCTION

Supercapacitors are attracting more and more interest due to their high power density and long-cycle life.[1,2] However, the low energy density seriously restricts their further application in the field of energy storage. Therefore, the development of high energy density electrode materials for supercapacitors has become a key problem to be solved.[3−5]

MoO_3 is considered as an excellent electrode material because of its high specific capacitance, low cost, and environmentally benign properties. Despite these advantages, pure MoO_3 suffers from a low electrical conductivity and poor cycle stability, and this inevitably limits its further application as an electrode material for electrochemical energy storage.[6,7]

The combination of MoO_3 with a high-conductivity material is an effective approach to solve these problems.[8] Yan et al. coupled MoO_3 with Ag nanoparticles to increase the conductivity of MoO_3-based electrodes. The as-prepared electrode showed a higher capacitance (225 F g^{-1}) compared with the MoO_3 electrode without Ag nanoparticles (69 F g^{-1}).[9] Faraji and Abedini demonstrated the fabrication of the MoO_3/GO/MWCNTs/graphite composite. The composite exhibits an excellent conductivity and a remarkable areal capacitance of 103 mF cm^{-2}.[10] However, although many efforts have been made to construct MoO_3-based composite electrodes, it remains a challenge to exploit composition rules for the design of high-performance composite electrodes.

In this work, polypyrrole (PPy) was applied to modify the conductivity of MnO_3 and provide additional pseudocapacitance for supercapacitors. In order to further improve the conductivity and cycle stability of the electrode material, reduced graphene oxide (rGO) was also used to construct a three-dimensionally (3D) interconnected conductive network via forming a high conductive coating layer on the surface of the MnO_3/PPy composite. Strong synergetic effects were observed between MoO_3, PPy, and rGO. Owing to the abovementioned advantages, the as-prepared composite exhibits a high specific capacitance (335 F g^{-1}, at 1 A g^{-1}) and a good cycling stability (remained 85.1%, at 2A g^{-1}, 6000 cycles). Moreover, the symmetric supercapacitor cell based on this composite shows a remarkable energy density (19.8 W h Kg^{-1}, at a power density of 301 W Kg^{-1}).

2. RESULTS AND DISCUSSION

The morphologies of the samples were characterized by scanning electron microscopy (SEM). As shown in Figure 1a, MoO_3 has a distinct wire-like structure, and the diameter of the MoO_3 nanowires (NWs) is about 100 nm. The rGO sheets in Figure 1b overlap each other to form a typical 3D network structure. Figure 1c is the SEM image of the MoO_3/PPy composite. As seen, PPy nanoparticles are uniformly attached

Received: December 7, 2020
Accepted: February 4, 2021
Published: March 29, 2021

https://doi.org/10.1021/acsomega.0c05953
ACS Omega 2021, 6, 9426−9432

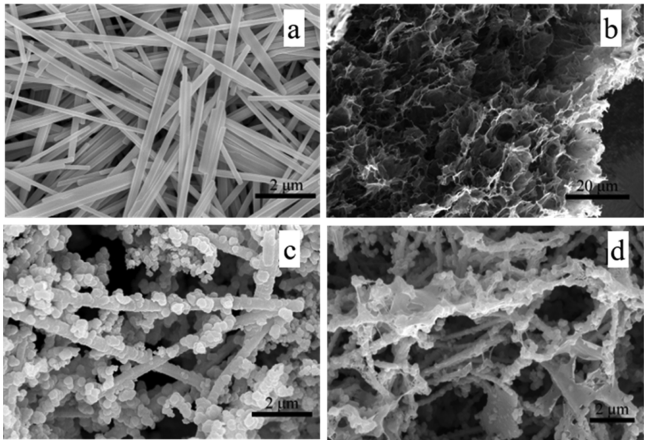

Figure 1. SEM images of (a) MoO_3 NWs, (b) rGO, (c) PPy/MoO_3, and (d) MoO_3/PPy/rGO.

to the surface of the MoO_3 NWs, and the composites shows a rough surface. Moreover, the average distance between two NWs in MoO_3/PPy has been increased obviously compared with that of pure MoO_3, indicating that PPy nanoparticles can efficiently prevent the agglomeration of MoO_3 NWs. This loose stacking structure can not only increase the electrode−electrolyte contact area but also provide more ion diffusion pathways. However, the large spacing between PPy nanoparticles may cause a low electrical conductivity. In Figure 1d, MoO_3/PPy is uniformly covered by rGO sheets to form an interconnected conductive network. Such a unique structure can efficiently increase the conductivity of the composite. Furthermore, the rGO coating can restrain the volume change in PPy nanoparticles and MoO_3 NWs during the charge and discharge process, leading to a good cyclic stability.

X-ray photoelectron spectroscopy (XPS) was carried out to investigate the chemical configuration of the MoO_3/PPy/rGO composites.[11−13] In Figure 2a, the survey XPS spectrum indicates that the composite consists of four elements: molybdenum, carbon, nitrogen, and oxygen. The high-resolution Mo 3d spectrum in Figure 2b shows two peaks at 232.6 and 235.7 eV which are consistent with the Mo $3d_{5/2}$ and Mo $3d_{3/2}$, respectively.[14] As shown in Figure 2c, the peaks at 398.3, 399.8, 400.9, and 402.2 eV are appointed to the =N−, −N−H, −N−H^+, and =N−H^+, correspondingly, originating from the synthesized PPy.[15] In Figure 2d, the characteristic peaks at 530.4, 531.3, and 532.90 eV are corresponded to Mo−O, C−O−Mo, and C=O, respectively.[16] The abovementioned results indicate that the MoO_3/PPy/rGO composite was successfully prepared.

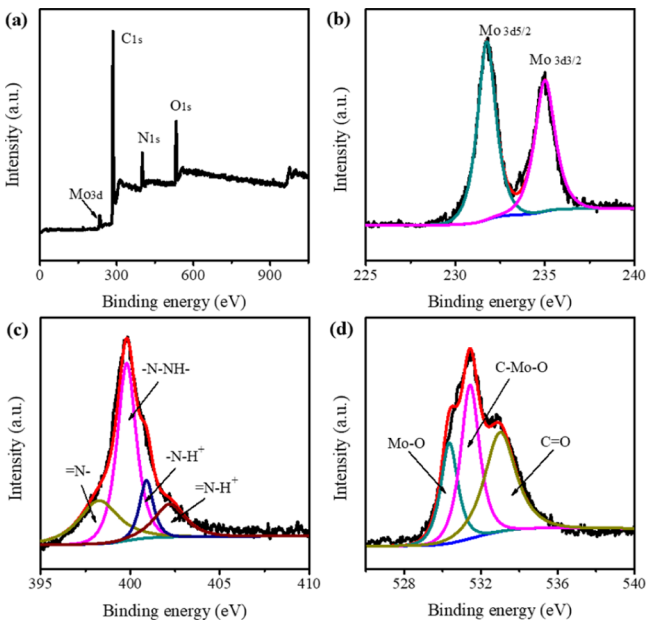

Figure 2. (a) XPS spectra of MoO_3/PPy/rGO; (b) corresponding high-resolution Mo 3d peak, (c) N 1s peak, and (d) O 1s peak.

Fourier transform infrared (FTIR) spectra were used to investigate the chemical structure of the samples. In Figure 3,

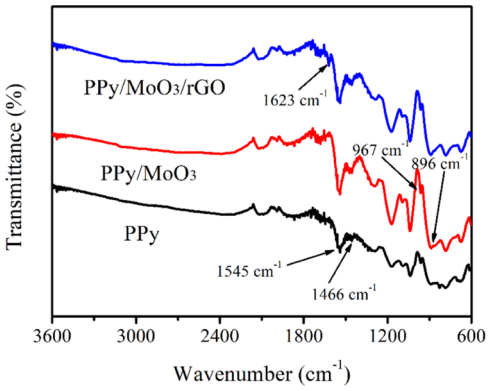

Figure 3. FTIR spectra of PPy, MoO_3/PPy, and MoO_3/PPy/rGO.

the FTIR spectrum of pure PPy displays two peaks at 1466 and 1545 cm^{-1}, which correspond to the C−N and C=C stretching vibration in the pyrrole ring, respectively.[17] In the spectrum of the PPy/MoO_3 composite, the characteristic peaks of MoO_3 appear at 967 and 896 cm^{-1}, which is consistent with those in the literature.[18] After the modification of rGO, a new peak is observed at 1623 cm^{-1}, which is assigned to the C=C stretching vibration of the graphene sheet.[10] Moreover, the characteristic peak of the O−H stretching at about 3500 cm^{-1} did not appear, indicating that the GO was successfully reduced.

The electrochemical performances of MoO_3 NWs, rGO, PPy, MoO_3/rGO, MoO_3/PPy, and MoO_3/PPy/rGO were investigated in a three-electrode cell. Figure 4a shows the comparative cyclic voltammetry (CV) curves of these six electrodes at a scan rate of 10 mV s^{-1}. The MoO_3/PPy/rGO shows the largest enclosed area than those of the other electrodes, suggesting a superior specific capacitance.[19] Moreover, except for the rGO electrode, the CV curves of the other electrodes are quasi-rectangles and have obvious redox peaks, originating from the pseudocapacitance behaviors of PPy and MoO_3.[1] Figure 4b displays the CV curves of the MoO_3/PPy/rGO electrode at scan rates ranging from 10 to 100 mV s^{-1}. The shape of the CV curves is changed gradually with increasing scan rates. It is caused by the fact that the electrolyte ions do not have enough time to diffuse into the inner sites of the electrode with high scan rates.[9] In order to further study the capacitive behavior of the samples, GCD tests were conducted at a current density of 1 A g^{-1}, and the results are presented in Figure 4c. As seen, the discharge times of these six electrodes increase in the order rGO < MoO_3 < MoO_3/rGO < PPy < MoO_3/PPy < MoO_3/PPy/rGO. This trend suggests that the specific capacitance of the MoO_3 can be improved via

https://doi.org/10.1021/acsomega.0c05953
ACS Omega 2021, 6, 9426−9432

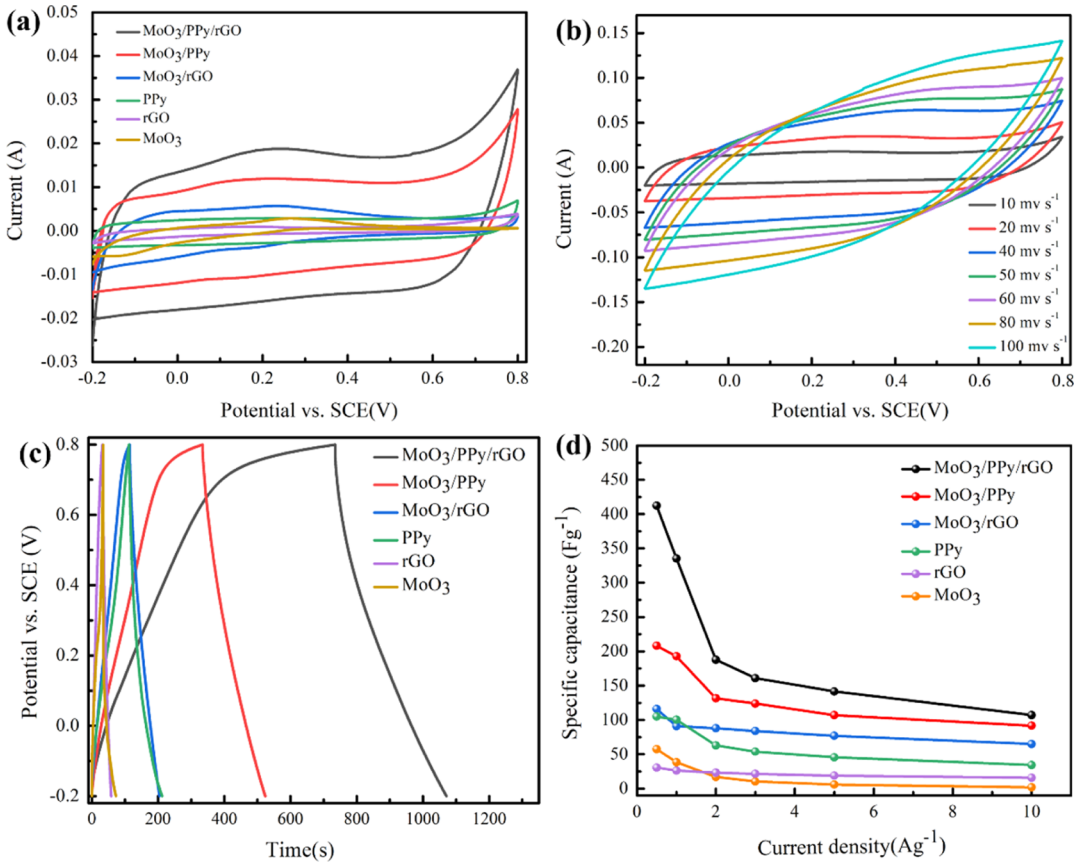

Figure 4. (a) CV curves of PPy, rGO, MoO_3, MoO_3/PPy, MoO_3/rGO, and MoO_3/PPy/rGO electrodes at a scan rate of 10 mV s^{-1}. (b) CV curves of the MoO_3/PPy/rGO electrode at scan rates from 10 to 100 mV s^{-1}. (c) GCD curves of PPy, rGO, MoO_3, MoO_3/PPy, MoO_3/rGO, and MoO_3/PPy/rGO electrodes at 1 A g^{-1}. (d) Specific capacitances of PPy, rGO, MoO_3, MoO_3/PPy, MoO_3/rGO, and MoO_3/PPy/rGO electrodes at current densities ranging from 0.5 to 10 A g^{-1}.

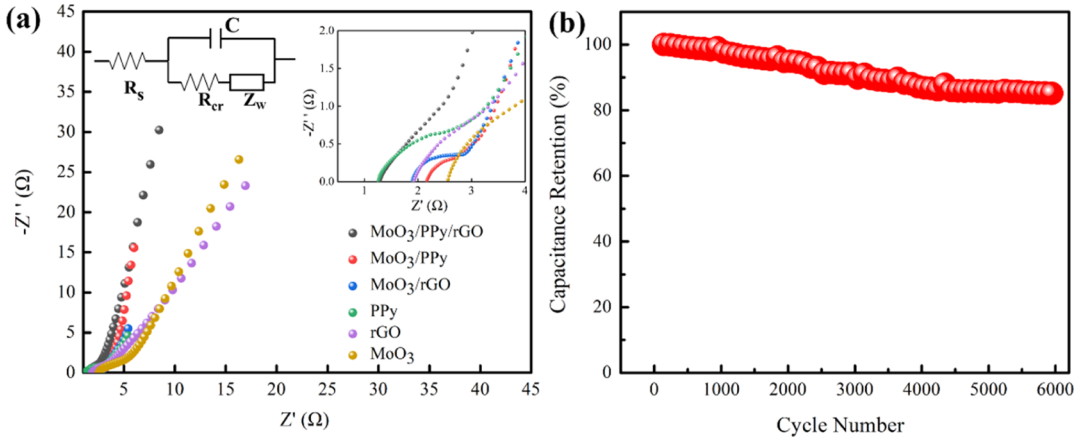

Figure 5. (a) EIS curves of PPy, rGO, MoO_3, MoO_3/PPy, MoO_3/rGO, and MoO_3/PPy/rGO electrodes. The inset of (a) is EIS curves of these electrodes in high-frequency regions and the equivalent circuit of the EIS spectra. (b) Cycling stability of PPy, rGO, MoO_3, MoO_3/PPy, MoO_3/rGO, and MoO_3/PPy/rGO electrodes for 6000 charge/discharge cycles at a current density of 2 A g^{-1}.

combining with PPy nanoparticles and rGO sheets. The relationships of the specific capacitances as a function of the current densities for these six electrodes are shown in Figure 4d. The highest specific capacitance of 412.3 F g^{-1} is obtained for the MoO_3/PPy/rGO electrode at a current density of 0.5 A g^{-1}, compared with specific capacitances of 30.7, 57.5, 105, 116, and 208.1 F g^{-1} for rGO, MoO_3, PPy, MoO_3/rGO, and MoO_3/PPy electrodes, respectively. Notably, the specific capacitance of the MoO_3/PPy/rGO electrode is evidently higher than the sum of the specific capacitances of the MoO_3/rGO electrode and MoO_3/PPy electrode. This may be due to the synergistic effect between MoO_3, PPy nanoparticles, and rGO sheets. Moreover, when the current density is increased to 10 A g^{-1}, the specific capacitance of the MoO3/PPy/rGO electrode remains as 107.3 F g^{-1}, still higher than those of the other electrodes at the same current density.

Electrochemical impedance spectroscopy (EIS) analysis was performed to further investigate the synergistic effect between

https://doi.org/10.1021/acsomega.0c05953
ACS Omega 2021, 6, 9426−9432

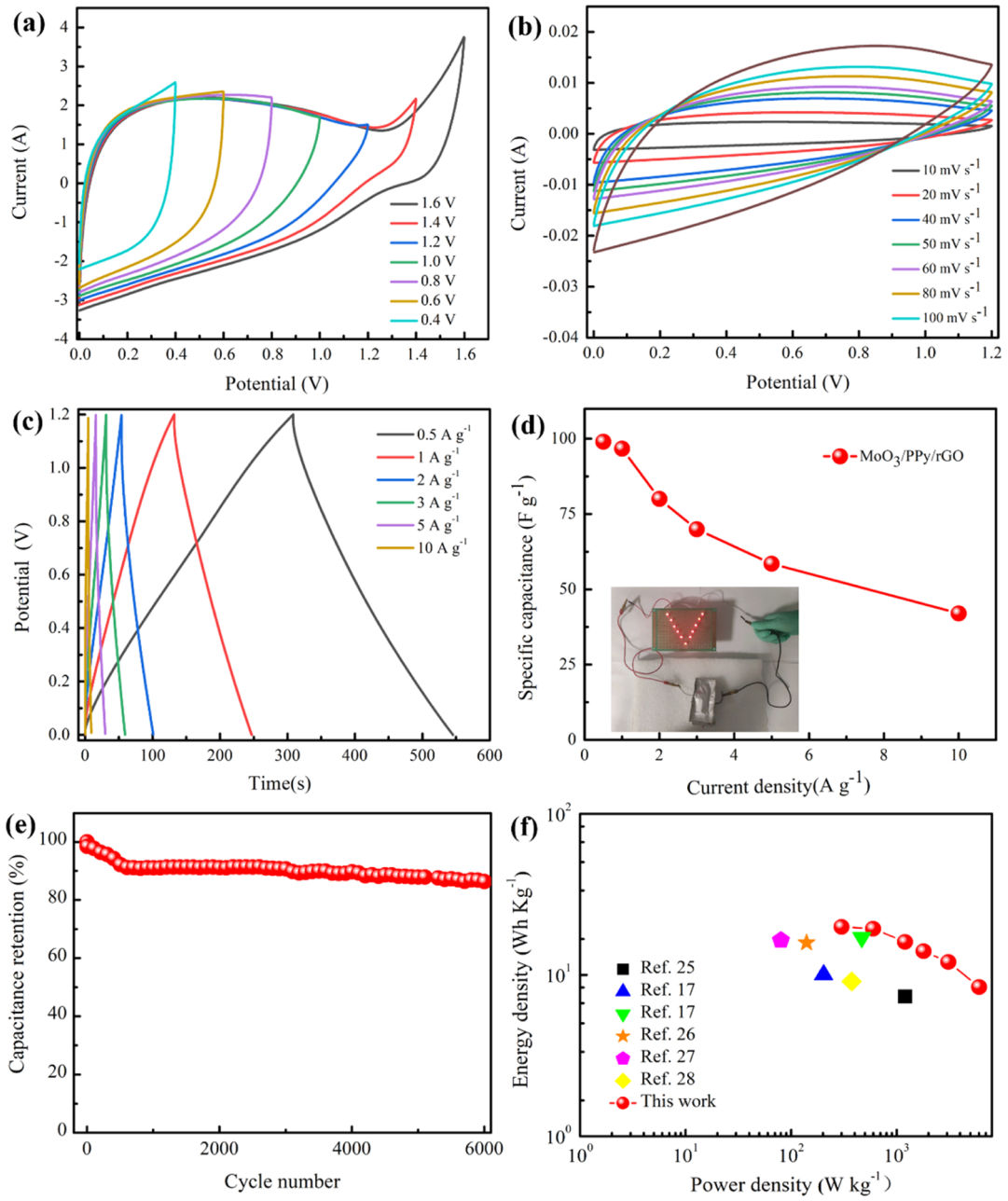

Figure 6. (a) CV curves of the MoO_3/PPy/rGO//MoO_3/PPy/rGO symmetric supercapacitor at different voltage ranges at a scan rate of 10 mV s^{-1}. (b) CV curves of the symmetric supercapacitor at different scan rates from 10 to 100 mV s^{-1}. (c) Galvanostatic charge/discharge (GCD) curves of the symmetric supercapacitor at various current densities. (d) Specific capacitance of the symmetric supercapacitor at various current densities. (e) Cycle performance of the symmetric supercapacitor at a current density of 2 A g^{-1}. (f) Ragone plots of the MoO_3/PPy/rGO// MoO_3/PPy/rGO symmetric supercapacitor in comparison to other supercapacitors from literature studies.

PPy nanoparticles and rGO sheets. The Nyquist plots of different samples are shown in Figure 5a. The inset is the equivalent circuit for the simulation of the EIS spectra. The internal resistance (R_s) values of MoO_3 NWs, rGO, PPy, MoO_3/rGO, MoO_3/PPy, and MoO_3/PPy/rGO electrodes are 2.6, 1.9, 1.3, 1.9, 2.2, and 1.3 Ω, respectively. The R_s of PPy is evidently lower than that of MoO3 and rGO. However, when PPy is combined with MoO_3, the R_s increases from 1.3 to 2.2, which may be due to the granular PPy which is difficult to connect with each other to form a conductive network in the composites. On the other hand, the R_s of rGO is 1.9 Ω, which is slightly higher than that of PPy. After being combined with MoO_3, the R_s of MoO_3/rGO is still 1.9 Ω, which is the same as that of the pristine rGO. This may be due to the fact that the rGO sheets with a high specific surface area easily form an interconnected conductive network on the surface of the MoO_3 NWs. It is worth noting that the R_s of the MoO_3/PPy/rGO electrode is as low as that of the pure PPy sample, which further proves that the synergistic effect between PPy nanoparticles and rGO sheets greatly enhances the conductivity of MoO_3/PPy/rGO. The charge transfer resistance (R_{ct}) values of MoO_3 NWs, rGO, PPy, MoO_3/rGO, MoO_3/PPy, and MoO_3/PPy/rGO electrodes are 0.45, 0.28, 0.29, 0.46, 0.01, and 0.01 Ω, respectively. The R_{ct} of the MoO_3/PPy and MoO_3/PPy/rGO electrode is negligible compared with that of the other electrode. This is due to the fact that the highly

https://doi.org/10.1021/acsomega.0c05953
ACS Omega 2021, 6, 9426−9432

conductive PPy nanoparticles acted as a conducting binder and promoted the electron transportation within the electrode.[20−22] The slope of the line in the low frequency range is indicative of the capacitive behavior of the active material.[23,24]

As seen, the MoO_3 electrode exhibits the lowest slop among these six electrodes. It may be due to the compact stacking structure of the MoO_3 NWs, which hinders the ions penetrating into the electrode pores. After being combined with PPy, the slope of the MoO_3/PPy composites increases obviously. It indicates that PPy nanoparticles can efficiently inhibit the aggregation of MoO_3 NWs. This result is also consistent with the SEM images mentioned above. Interestingly, the slope of the MoO_3/PPy/rGO electrode is slightly lower than that of MoO_3/PPy. This is because the coating layer formed by rGO sheets hindered the diffusion of ions. The cycling stability of MoO_3/PPy/rGO was also studied, and the result is shown in Figure 5b. After 6000 charge and discharge cycles at a current density of 2 A g^{-1}, the capacitance retention of MoO_3/PPy/rGO was 85.1%. This good cycling stability should be attributed to the rGO sheets acting as a protective layer to prevent the volume expansions of the MoO_3 and PPy during the charge/discharge process.[8]

In order to further study the practical application performance of the MoO_3/PPy/rGO material, a symmetric supercapacitor made up of two MoO_3/PPy/rGO electrodes was assembled. Figure 6a displays the CV curves of the MoO_3/PPy/rGO//MoO_3/PPy/rGO supercapacitor at different voltage ranges at a scan rate of 10 mV s^{-1}. The curve keeps its rectangular shape even with a 1.2 V voltage range, suggesting a good cycle reversibility.[25] According to the abovementioned test results, the electrochemical properties of the MoO_3/PPy/rGO//MoO_3/PPy/rGO symmetric supercapacitor were tested in the voltage window of 0−1.2 V. Figure 6b shows the CV curves of the symmetric supercapacitor at different scan rates. The curves at low scan rates show distorted rectangular shapes, suggesting the pseudocapacitance characteristics of the MoO_3 and PPy. The charge/discharge curves at various current densities are exhibited in Figure 6c. The curves present ideal linear behaviors even at a high current density of 10 A g^{-1}, indicating that the symmetric supercapacitor has excellent rate capability.[26] The specific capacitances of the symmetric supercapacitor at various current densities are calculated from the discharge curves and shown in Figure 6d. The specific capacity is 99 F g^{-1} at a current density of 0.5 A g^{-1}. As the current density increases to 10 A g^{-1}, the specific capacity decreases from 99 to 42 F g^{-1}. The excellent practical performance is demonstrated by lightning an LED device, as shown in the Figure 6d inset. As shown in Figure 6e, the capacitance retention of the symmetric supercapacitor was 86.2% after 6000 cycles at a current density of 2 A g^{-1}, suggesting a good cycling stability. Ragone plots of the MoO_3/PPy/rGO//MoO_3/PPy/rGO symmetric supercapacitor are presented in Figure 6f. The symmetric supercapacitor exhibits a remarkable energy density of 19.8 W h kg^{-1} at a power density of 301 W kg^{-1}, superior to those of other reported materials for supercapacitors, for instance, microrods architectured MoO_3 (7.33 W h kg^{-1}, 1200 W kg^{-1}),[27] MoS_2/MoO_3/PPy (10 W h kg^{-1}, 203 W kg^{-1}),[19] symmetric PPy/N-doped graphene (17 W h kg^{-1} at 467 W kg^{-1}),[19] PPy-rGO composites (15.8 W h kg^{-1}, 140 W kg^{-1}),[28] PPy-GO composites (16.4 W h kg^{-1}, 80 W kg^{-1}),[29] and PPy-rG// PPy-rG (9.1 W h kg^{-1}, 375 W kg^{-1}).[30]

3. CONCLUSIONS

In this work, we have successfully designed and synthesized a 3D networked MoO_3/PPy/rGO composite via a facile three-step method. The as-prepared electrode exhibits an excellent specific capacity of 412.3 F g^{-1} at a current density of 0.5 A g^{-1} and a good cycling stability (remained 85.1% after 6000 cycles at 2 A g^{-1}). The remarkable performances of the MoO_3/PPy/rGO electrode are attributed to the following reasons: (i) PPy nanoparticles can efficiently prevent the agglomeration of MoO3 NWs, and this can not only provide more electrochemical active sites but also offer shortened pathways for ions; (ii) MoO_3 NWs are covered with a high conductive layer composed of PPy nanoparticles and rGO sheets, and this unique structure significantly reduces the R_s and R_{ct} of the composite; (iii) the rGO coating can prevent the volume change in the MoO_3/PPy composite during charge/discharge cycles, leading to an excellent long-term cycle stability. Furthermore, the symmetric supercapacitor based on the MoO_3/PPy/rGO electrode shows a high energy density (19.8 W h Kg^{-1}, at a power density of 301 W Kg^{-1}) and good cycling stability of 86.2% capacitance retention after 6000 cycles. These results demonstrate that the MoO_3/PPy/rGO composite is a promising material for high-performance supercapacitor.

4. EXPERIMENTAL SECTION

4.1. Materials. Ammonium molybdate [$(NH_4)_6Mo_7O_{24}\cdot 4H_2O$, AR], nitric acid ($HNO_3$, 65%), ammonium persulphate ($(NH_4)_2S_2O_4$, AR], and the pyrrole monomer (AR grade) were purchased from Aladdin Reagent Co. Ltd. (China). rGO was purchased from XFNANO Materials Tech Co. Ltd. (Nanjing, China). The whole experiment process used deionized (DI) water. All of the reagents are analytically pure without further purification.

4.2. Material Characterization. Field-emission scanning electron microscopy was performed on a Hitachi S-4800 scanning electron microscope. XPS measurements were carried out on a Thermo Fisher X-ray photoelectron spectrometer equipped with Al radiation as the probe (Kα, radiation), with a chamber pressure of 5×10^{-9} Torr. The analysis spot size was 400 μm in diameter. The chemical structure of the samples was investigated using FTIR spectrometer (Nicolet6700, Thermofisher).

4.3. Electrochemical Tests. Whole electrochemical tests in this work were carried out on a CHI660E workstation (Shanghai Chenhua) in 1 mol L^{-1} Na_2SO_4 aqueous solution. A three-electrode system was used to investigate the electrochemical performance of the samples. A saturated calomel electrode and Pt wire served as the reference and counter electrode, respectively. The working electrodes were fabricated by compressing the active materials onto nickel foams. A two-electrode system was used to study the electrochemical properties of the symmetric supercapacitor constructed by assembling two same PPy/GO/MoO_3 electrodes in 1 mol L^{-1} Na_2SO_4 aqueous electrolyte. The symmetric supercapacitor is named PPy/GO/MnO_3//PPy/GO/MnO_3.

The specific capacitances (C_s) of the individual electrode and the two-electrode cell were calculated from the galvanostatic discharge curves using eq 1. The specific energy density (E_c) and specific power density (P_c) were calculated according to equation 2 and equation 3, respectively

https://doi.org/10.1021/acsomega.0c05953
ACS Omega 2021, 6, 9426−9432

Scheme 1. Schematic Diagram of the Fabrication Process of the MoO_3/PPy/rGO Composite

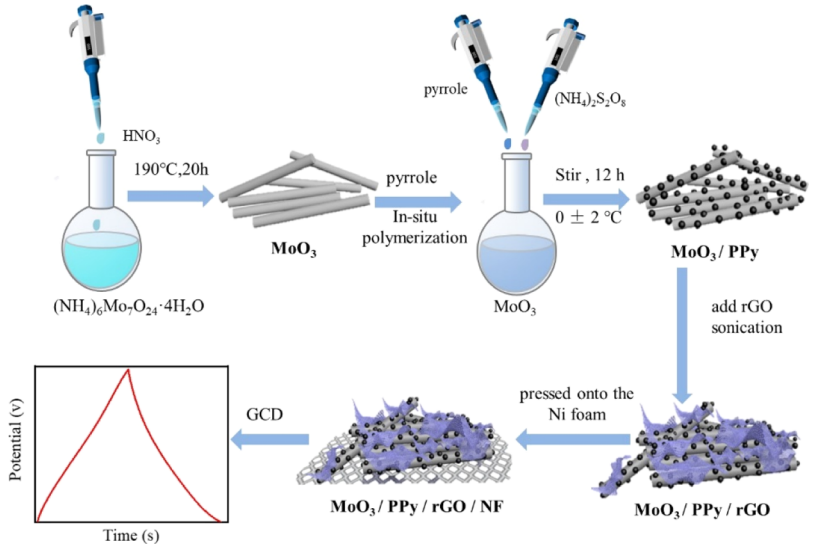

$$C_s = \frac{I\Delta t}{m\Delta U} \quad (1)$$

$$E_c = \frac{C_s \Delta U^2}{2 \times 3.6} \quad (2)$$

$$P_c = \frac{E_c \times 3600}{\Delta t} \quad (3)$$

where I is the discharge current, Δt is the discharge time, m is the mass of the active material in the three-electrode system and in the two-electrode cell, m is the total active mass of both electrodes, and ΔU is the voltage window.

4.4. Synthesis of MoO_3 NWs. $(NH_4)_6Mo_7O_{24}{\cdot}4H_2O$ (1.3 g) was dissolved fully in 50 mL of DI water and stirred. 65% HNO_3 was used to adjust the pH of the solution to 1.0. Then, the solution was transferred into a 150 mL Teflon-lined stainless-steel autoclave with heat at 185 °C for 15 h. Finally, the product was obtained by centrifuging and washing with DI water and then dried at 55 °C in vacuum.

4.5. Synthesis of the MoO_3/PPy Composite. In situ oxidative polymerization of pyrrole was carried out with the MoO_3 template to obtain the MoO_3/PPy composite. The $(NH_4)_2S_2O_4$ served as an oxidant. MoO_3 NWs (21 mg) were added in 90 mL of DI water and stirred. Then, 210 μL of pyrrole was added with an ice bath. Two hours later, 21 mL of $(NH_4)_2S_2O_4$ solution was added dropwise. The mole ratio of pyrrole and $(NH_4)_2S_2O_4$ was 2:1. After 10 h of ice bath reaction, the sediments were collected by centrifuging and washing with DI water and dried in vacuum at 55 °C for 10 h.

4.6. Preparation of the MoO_3/PPy/rGO Composite. MoO_3-PPy NWs (15 mg) were put into a round bottom flask and dispersed in 40 mL of DI water by sonication. Subsequently, 5 mg of rGO was added to the suspension and continued to sonicate for 40 min. The product was centrifuged and washed with DI water and absolute ethanol five times. Finally, the product was transferred into a vacuum drying oven and dried for 6 h at 65 °C. The schematic diagram of the composite material is shown in Scheme 1.

AUTHOR INFORMATION

Corresponding Authors

Dejuan Huang − *Jiangxi Province Key Laboratory of Polymer Micro/Nano Manufacturing and Devices, School of Chemistry, Biology, and Materials Science, East China University, Nanchang, Jiangxi 330013, China*; Email: djhuang@ecut.edu.cn

Tianxiang Jin − *Jiangxi Province Key Laboratory of Polymer Micro/Nano Manufacturing and Devices, School of Chemistry, Biology, and Materials Science, East China University, Nanchang, Jiangxi 330013, China*; orcid.org/0000-0001-5950-6792; Phone: 0086 15797729785; Email: 201660027@ecut.edu.cn

Authors

Hangchun Deng − *Jiangxi Province Key Laboratory of Polymer Micro/Nano Manufacturing and Devices, School of Chemistry, Biology, and Materials Science, East China University, Nanchang, Jiangxi 330013, China*

Jie Huang − *Jiangxi Province Key Laboratory of Polymer Micro/Nano Manufacturing and Devices, School of Chemistry, Biology, and Materials Science, East China University, Nanchang, Jiangxi 330013, China*

Zhiyong Hu − *Jiangxi Province Key Laboratory of Polymer Micro/Nano Manufacturing and Devices, School of Chemistry, Biology, and Materials Science, East China University, Nanchang, Jiangxi 330013, China*

Xiangfei Chen − *Jiangxi Province Key Laboratory of Polymer Micro/Nano Manufacturing and Devices, School of Chemistry, Biology, and Materials Science, East China University, Nanchang, Jiangxi 330013, China*

Complete contact information is available at: https://pubs.acs.org/10.1021/acsomega.0c05953

Notes

The authors declare no competing financial interest.

ACKNOWLEDGMENTS

The authors thank the financial support by the Foundation of Jiangxi Educational Committee (GJJ170427 and GJJ170437), the NSF of Jiangxi (20181BAB203012), and East China

https://doi.org/10.1021/acsomega.0c05953
ACS Omega 2021, 6, 9426−9432

University of Technology Research Foundation for Advanced Talents no. DHBK2016110.

REFERENCES

(1) Chen, J.; Lin, C.; Zhang, M.; Jin, T.; Qian, Y. Constructing Nitrogen, Selenium Co-Doped Graphene Aerogel Electrode Materials for Synergistically Enhanced Capacitive Performance. *ChemElectroChem* **2020**, *7*, 3311−3318.
(2) Wang, Y.; Zhang, L.; Hou, H.; Xu, W.; Duan, G.; He, S.; Liu, K.; Jiang, S. Recent progress in carbon-based materials for supercapacitor electrodes: a review. *J. Mater. Sci.* **2020**, *56*, 173−200.
(3) Akhtar, A. J.; Mishra, S.; Saha, S. K. Charge transport mechanism in reduced graphene oxide/polypyrrole based ultrahigh energy density supercapacitor. *J. Mater. Sci.* **2020**, *31*, 11637−11645.
(4) Ke, Q.; Wang, J. Graphene-based materials for supercapacitor electrodes - A review. *J. Materiomics* **2016**, *2*, 37−54.
(5) Li, Q.; Xia, Y.; Wan, X.; Yang, S.; Cai, Z.; Ye, Y.; Li, G. Morphology-dependent MnO2/nitrogen-doped graphene nanocomposites for simultaneous detection of trace dopamine and uric acid. *Mater. Sci. Eng., C* **2020**, *109*, 110615.
(6) Wang, Q.; Zhou, C.; Yan, X.; Wang, J.; Wang, D.; Yuan, X.; Cheng, X. One-dimensional MoO3 coated by carbon for supercapacitor with enhanced electrochemical performance. *J. Mater. Sci.* **2019**, *30*, 6643−6649.
(7) Mendoza-Sánchez, B.; Brousse, T.; Ramirez-Castro, C.; Nicolosi, V.; Grant, P. S. An investigation of nanostructured thin film α-MoO_3 based supercapacitor electrodes in an aqueous electrolyte. *Electrochim. Acta* **2013**, *91*, 253−260.
(8) Li, G.; Xia, Y.; Tian, Y.; Wu, Y.; Liu, J.; He, Q.; Chen, D. Review-Recent Developments on Graphene-Based Electrochemical Sensors toward Nitrite. *J. Electrochem. Soc.* **2019**, *166*, B881−B895.
(9) Zhou, C.; Wang, Q.; Yan, X. H.; Wang, J. J.; Wang, D. F.; Yuan, X. X.; Jiang, H.; Zhu, Y. H.; Cheng, X. N. A facile route to synthesize Ag decorated MoO3 nanocomposite for symmetric supercapacitor. *Ceram. Int.* **2020**, *46*, 15385−15391.
(10) Faraji, M.; Abedini, A. Fabrication of electrochemically interconnected MoO_3/GO/MWCNTs/graphite sheets for high performance all-solid-state symmetric supercapacitor. *Int. J. Hydrogen Energy* **2019**, *44*, 2741−2751.
(11) Zhu, M.; Shao, Q.; Pi, Y.; Guo, J.; Huang, B.; Qian, Y.; Huang, X. Ultrathin Vein-Like Iridium-Tin Nanowires with Abundant Oxidized Tin as High-Performance Ethanol Oxidation Electrocatalysts. *Small* **2017**, *13*, 1701295.
(12) Zhu, M.; Shao, Q.; Qian, Y.; Huang, X. Superior overall water splitting electrocatalysis in acidic conditions enabled by bimetallic Ir-Ag nanotubes. *Nano Energy* **2019**, *56*, 330−337.
(13) Zhu, T.; Ding, J.; Shao, Q.; Qian, Y.; Huang, X. P,Se-Codoped MoS2 Nanosheets as Accelerated Electrocatalysts for Hydrogen Evolution. *ChemCatChem* **2019**, *11*, 689−692.
(14) Bica de Moraes, M. A.; Trasferetti, B. C.; Rouxinol, F. P.; Landers, R.; Durrant, S. F.; Scarmínio, J.; Urbano, A. Molybdenum Oxide Thin Films Obtained by the Hot-Filament Metal Oxide Deposition Technique. *Chem. Mater.* **2004**, *16*, 513−520.
(15) Šetka, M.; Calavia, R.; VojkuÅvka, L.; Llobet, E.; Drbohlavová, J.; Vallejos, S. Raman and XPS studies of ammonia sensitive polypyrrole nanorods and nanoparticles. *Sci. Rep.* **2019**, *9*, 8465.
(16) Liu, X.; Liu, Y.; Yan, X.; Lan, J.-L.; Yu, Y.; Yang, X. Ultrafine MoO_3 nanoparticles embedded in porous carbon nanofibers as anodes for high-performance lithium-ion batteries. *Mater. Chem. Front.* **2019**, *3*, 120−126.
(17) Ramesan, M. T.; Santhi, V.; Bahuleyan, B. K.; Al-Maghrabi, M. A. Structural characterization, material properties and sensor application study of in situ polymerized polypyrrole/silver doped titanium dioxide nanocomposites. *Mater. Chem. Phys.* **2018**, *211*, 343−354.
(18) Subba Reddy, C. V.; Qi, Y. Y.; Jin, W.; Zhu, Q. Y.; Deng, Z. R.; Chen, W.; Mho, S.-i. An electrochemical investigation on (MoO3+PVP+PVA) nanobelts for lithium batteries. *J. Solid State Electrochem.* **2007**, *11*, 1239−1243.
(19) Sari, F. N. I.; Ting, J.-M. High performance asymmetric supercapacitor having novel 3D networked polypyrrole nanotube/N-doped graphene negative electrode and core-shelled MoO_3/PPy supported MoS2 positive electrode. *Electrochim. Acta* **2019**, *320*, 134533.
(20) Li, J.; Yun, X.; Hu, Z.; Xi, L.; Li, N.; Tang, H.; Lu, P.; Zhu, Y. Three-dimensional nitrogen and phosphorus co-doped carbon quantum dots/reduced graphene oxide composite aerogels with a hierarchical porous structure as superior electrode materials for supercapacitors. *J. Mater. Chem. A* **2019**, *7*, 26311−26325.
(21) Yuan, Y.; Lv, H.; Xu, Q.; Liu, H.; Wang, Y. A few-layered MoS2 nanosheets/nitrogen-doped graphene 3D aerogel as a high performance and long-term stability supercapacitor electrode. *Nanoscale* **2019**, *11*, 4318−4327.
(22) Cai, Z.; Ye, Y.; Wan, X.; Liu, J.; Yang, S.; Xia, Y.; Li, G.; He, Q. Morphology-Dependent Electrochemical Sensing Properties of Iron Oxide-Graphene Oxide Nanohybrids for Dopamine and Uric Acid. *Nanomaterials* **2019**, *9*, 835.
(23) Li, Y.; Wang, G.; Wei, T.; Fan, Z.; Yan, P. Nitrogen and sulfur co-doped porous carbon nanosheets derived from willow catkin for supercapacitors. *Nano Energy* **2016**, *19*, 165−175.
(24) Liu, H.; Xiong, R.; Zhong, P.; Li, G.; Liu, J.; Wu, J.; Liu, Y.; He, Q. Nanohybrids of shuttle-like α-Fe_2O_3 nanoparticles and nitrogen-doped graphene for simultaneous voltammetric detection of dopamine and uric acid. *New J. Chem.* **2020**, *44*, 20797−20805.
(25) Lee, J.-S. M.; Briggs, M. E.; Hu, C.-C.; Cooper, A. I. Controlling electric double-layer capacitance and pseudocapacitance in heteroatom-doped carbons derived from hypercrosslinked microporous polymers. *Nano Energy* **2018**, *46*, 277−289.
(26) Seevakan, K.; Manikandan, A.; Devendran, P.; Baykal, A.; Alagesan, T. Electrochemical and magneto-optical properties of cobalt molybdate nano-catalyst as high-performance supercapacitor. *Ceram. Int.* **2018**, *44*, 17735−17742.
(27) Pujari, R. B.; Lokhande, V. C.; Kumbhar, V. S.; Chodankar, N. R.; Lokhande, C. D. Hexagonal microrods architectured MoO_3 thin film for supercapacitor application. *J. Mater. Sci.* **2016**, *27*, 3312.
(28) Zhu, J.; Feng, T.; Du, X.; Wang, J.; Hu, J.; Wei, L. High performance asymmetric supercapacitor based on polypyrrole/graphene composite and its derived nitrogen-doped carbon nanosheets. *J. Power Sources* **2017**, *346*, 120−127.
(29) Cao, J.; Wang, Y.; Chen, J.; Li, X.; Walsh, F. C.; Ouyang, J.-H.; Jia, D.; Zhou, Y. Three-dimensional graphene oxide/polypyrrole composite electrodes fabricated by one-step electrodeposition for high performance supercapacitors. *J. Mater. Chem. A* **2015**, *3*, 14445−14457.
(30) Cai, X.; Lim, S. H.; Poh, C. K.; Lai, L.; Lin, J.; Shen, Z. High-performance asymmetric pseudocapacitor cell based on cobalt hydroxide/graphene and polypyrrole/graphene electrodes. *J. Power Sources Adv.* **2015**, *275*, 298−304.

https://doi.org/10.1021/acsomega.0c05953
ACS Omega 2021, 6, 9426−9432